Multi-scale gyrokinetic simulations: Comparison with experiment and implications for predicting turbulence and transport

N. T. Howard' , C. Holland, A. E. White, M. Greenwald, J. Candy, and A. J. Creely

Articles you may be interested in

Synergistic cross-scale coupling of turbulence in a tokamak plasma
Physics of Plasmas **21**, 112510112510 (2014); 10.1063/1.4902366

Validation of nonlinear gyrokinetic simulations of L- and I-mode plasmas on Alcator C-Mod
Physics of Plasmas **24**, 056104056104 (2017); 10.1063/1.4977466

Validation metrics for turbulent plasma transport
Physics of Plasmas **23**, 060901060901 (2016); 10.1063/1.4954151

The role of zonal flows in the saturation of multi-scale gyrokinetic turbulence
Physics of Plasmas **23**, 062518062518 (2016); 10.1063/1.4954905

Multi-scale gyrokinetic simulation of Alcator C-Mod tokamak discharges
Physics of Plasmas **21**, 032308032308 (2014); 10.1063/1.4869078

Role of density gradient driven trapped electron mode turbulence in the H-mode inner core with electron heating
Physics of Plasmas **23**, 056112056112 (2016); 10.1063/1.4948723

Multi-scale gyrokinetic simulations: Comparison with experiment and implications for predicting turbulence and transport

N. T. Howard,[1,a),b)] C. Holland,[2] A. E. White,[1] M. Greenwald,[1] J. Candy,[3] and A. J. Creely[1]

[1]*MIT - Plasma Science and Fusion Center, Cambridge, Massachusetts 02139, USA*
[2]*University of California - San Diego, La Jolla, California 92093, USA*
[3]*General Atomics, P.O. Box 85608, San Diego, California 92186, USA*

To better understand the role of cross-scale coupling in experimental conditions, a series of multi-scale gyrokinetic simulations were performed on Alcator C-Mod, L-mode plasmas. These simulations, performed using all experimental inputs and realistic ion to electron mass ratio ($(m_i/m_e)^{1/2} = 60.0$), simultaneously capture turbulence at the ion ($k_\theta \rho_s \sim \mathcal{O}(1.0)$) and electron-scales ($k_\theta \rho_e \sim \mathcal{O}(1.0)$). Direct comparison with experimental heat fluxes and electron profile stiffness indicates that Electron Temperature Gradient (ETG) streamers and strong cross-scale turbulence coupling likely exist in both of the experimental conditions studied. The coupling between ion and electron-scales exists in the form of energy cascades, modification of zonal flow dynamics, and the effective shearing of ETG turbulence by long wavelength, Ion Temperature Gradient (ITG) turbulence. The tightly coupled nature of ITG and ETG turbulence in these realistic plasma conditions is shown to have significant implications for the interpretation of experimental transport and fluctuations. Initial attempts are made to develop a "rule of thumb" based on linear physics, to help predict when cross-scale coupling plays an important role and to inform future modeling of experimental discharges. The details of the simulations, comparisons with experimental measurements, and implications for both modeling and experimental interpretation are discussed. *Published by AIP Publishing.* [http://dx.doi.org/10.1063/1.4946028]

I. INTRODUCTION

With the growing costs and engineering complexity associated with the next generation of fusion reactors, the need for reliable prediction of reactor performance, to both inform design and operation of such devices, becomes increasingly important. In the field of core plasma turbulence, great progress has been made in validating the nonlinear gyrokinetic model, to the point where it is now routinely applied to both interpret and predict experiments.[1–14] Most gyrokinetic research has focused on turbulence associated with long wavelength ($k_\theta \rho_s < 1.0$) electrostatic drift-wave modes such as the Ion Temperature Gradient (ITG) and Trapped Electron Modes (TEMs). Here, k_θ is the poloidal wavenumber, $\rho_s = c_s / \Omega_{c,i}$ is the ion gyroradius evaluated with the ion sound speed, $c_s = \sqrt{T_e/m_i}$ is the ion sound speed, and $\Omega_{c,i} = eB/m_i$ is the ion gyro-frequency. However, the discovery that short wavelength ($k_\theta \rho_s > 1.0$) Electron Temperature Gradient (ETG) mode turbulence can form radially elongated structures known as ETG streamers[15,16] has motivated its investigation as a serious candidate for explaining "anomalous" electron heat transport.

Years of research have focused on explaining experimental levels of ion and electron heat transport in the tokamak core using single-scale (ion or electron-scale) gyrokinetic simulation. However, to study the coupling of ion and electron-scale turbulence, multi-scale gyrokinetic simulation, capable of capturing the spatio-temporal dynamics associated with the electron and ion-scales simultaneously ($k_\theta \rho_s \sim 0.1$–60.0) is required. Such simulations push the limits of current supercomputing facilities, requiring large computing allocations, small simulation time steps, fine radial grids, and large simulation box sizes to capture the wide range of turbulent scales. To date, most multi-scale work has focused on the use of reduced electron mass ratio simulation.[17–23] Such simulations use artificially heavy electrons to reduce the gap between the electron and ion scales, making the computation more tractable. Unfortunately, this approximation also limits the applicability of experimental comparisons.[24] The coupling of ion and electron-scale turbulence in experimental plasma conditions has only recently[25,26] been investigated in a self consistent manner with a realistic ratio of ion to electron mass.

In this paper, we report a series of results from realistic electron mass, multi-scale gyrokinetic simulations of Alcator C-Mod discharges. The remainder of this paper is organized as follows: Section II provides a description of the experimental discharges studied and the numerical setup used for the nonlinear simulations. Section III focuses on multi-scale simulation of a low input power discharge, where transport results from previous work are summarized, new insights into cross-scale turbulence coupling are presented, and two new multi-scale simulations are discussed. Section IV describes multi-scale simulation of a high input power L-mode discharge, pointing out the similarities and differences with the low power condition studied. Section V attempts to identify signatures of ETG and implications of cross-scale coupling for experimental interpretation. Section VI presents a

first attempt at developing a linear stability based, "rule of thumb" for predicting when cross-scale coupling may be significant, and Section VII includes a summary and conclusions.

II. EXPERIMENTAL DESCRIPTION AND SIMULATION SETUP

The work presented here focuses on analysis from two Alcator C-Mod, L-mode discharges performed with effectively identical engineering parameters ($B_T = 5.4$ T; $I_p = 0.8$ MA; $n_e(0) \sim 1.4 \times 10^{20}$ m^{-3}) but with two levels of ion cyclotron heating (ICRH) at 1.2 MW and 3.5 MW. We will refer to these discharges as the low-power and high-power discharges throughout the text. These discharges have been studied extensively, and additional details of the experimental measurements, discharge parameters, and ion-scale simulation results can be found in Refs. 27 and 28.

All simulations presented in this paper were performed with the GYRO code.[29] GYRO is an Euerlian gyrokinetic code, used in numerous works for direct comparison with experiment.[2–4,8,27] Simulations presented here were local (performed at r/a = 0.6; normalized midplane minor radius), nonlinear, included 3 gyrokinetic species (deuterium, electrons, and boron—the dominant impurity species in C-Mod discharges), realistic ion to electron mass ($\mu = (m_i/m_e)^{1/2} = 60.0$), rotation effects (E × B shear, Coriolis drift effects, and parallel flow gradients), electron-ion collisions, Miller geometry,[30] and a 128 point velocity space discretization (8 energies, 8 pitch angles, 2 signs of velocity). Given the low beta of the discharges studied ($\beta_e \sim 0.1\%$), all simulations were electrostatic. Multi-scale simulations utilized 342 complex toroidal modes with $\Delta n = 18$ to span from $\sim k_\theta \rho_s = 0.14$–48.0 ($\sim k_\theta \rho_e = 0.8$) with 1800 radial grid points used in the radial direction. Simulation box sizes were $60 \times 44 \rho_s$, in the radial and binormal directions including $8\rho_s$ radial buffer regions, used to implement the rotation effects in GYRO (further details can be found in Ref. 29). With these box sizes and the specified radial grid points, a resolution of $2\rho_e$ was used, consistent with the previous work.[18–20,25,26] Multi-scale simulations were typically performed for $\sim 425 a/c_s$ with time averaged quantities reported here were obtained from time averages over windows 150–200a/c_s long for multi-scale simulations. To ease comparison between the multi-scale and ion-scale results, the ion-scale simulation results (spanning up to $\sim k_\theta \rho_s = 1.25$) in this paper were obtained from simulations with identical box size ($60 \times 44 \rho_s$), typically utilizing 240 radial grid points.

Due to the extreme computational requirements of the multi-scale simulation, convergence tests were generally performed on the corresponding ion-scale simulations, including studies of radial resolution, velocity space, box size, and buffer regions. To ensure accurate results, it was confirmed that the chosen box size can sufficiently reproduce heat fluxes and heat flux spectra obtained from much larger, $128 \times 112 \rho_s$ ($8\rho_s$ buffers) simulations. Additionally, a single box size convergence was performed using multi-scale simulation where it was confirmed that $44 \times 32 \rho_s$ ($6\rho_s$ buffers) boxes could reproduce results obtained from $60 \times 44 \rho_s$ simulation boxes for the

conditions simulated. As a check to ensure the results obtained from ion-scale simulation were not affected by the radial resolution, a series ion-scale simulations with extremely high radial resolutions of 0.12 and $0.06\rho_s$ were also performed (using 500 and 1000 radial grid points, respectively). The overall approach for the simulations, including justification for the maximum simulated values of $k_\theta \rho_s$, has been documented here,[24] and the simulation input parameters can be found in Table I. A total of 8 multi-scale simulations are presented in this work. The computing time requirements for these simulations were approximately 125M CPU hours on the NERSC Hopper and Edison supercomputers.

III. MULTI-SCALE SIMULATION AND CROSS-SCALE COUPLING IN A LOW-POWER, L-MODE PLASMA

The first gyrokinetic model validation utilizing multi-scale gyrokinetic simulation was recently reported.[26] This work included 6 total multi-scale simulations, a 3 point scan of the ITG drive term (a/L_{T_i}), and a 3 point scan of the ETG drive term (a/L_{T_e}) within experimental uncertainties to demonstrate quantitative agreement between experimental Q_i, Q_e and electron profile stiffness. To provide the reader with context for the remainder of the paper, we summarize the transport results from this work before moving to new analysis.

A. A summary of transport changes found in multi-scale simulation

In order to probe the cross-scale coupling of the low power discharge, a 3 point scan of the ITG drive term (a/L_{T_i}) was performed using multi-scale gyrokinetic simulation. These results (reported in Ref. 26), in addition to a new multi-scale simulation point, are presented in Figure 1. An example of the electron heat flux spectra obtained from the $a/L_{T_i} = 1.92$ point of the scan is plotted in Figure 2 to demonstrate the importance of both the ion and electron-scales in these simulations. Near marginal stability for the ITG, multi-scale simulation displayed higher values of low-k ($k_\theta \rho_s < 1.0$) driven, Q_i and Q_e, leading to reduced ion stiffness ($dQ_i/d(a/L_{T_i})$). Such enhancement of the low-k heat fluxes was shown to be the direct result of increased fluctuation levels at ion-scales in multi-scale simulation[25] with similar observations of low-k enhancement later reported for CYCLONE base case parameters.[23] Extrapolation of multi-scale Q_i results in Figure 1 to the x-axis suggests that a reduced ITG critical gradient exists in multi-scale simulation relative to the corresponding ion-scale simulations. For conditions with strongly unstable ITG ($\sim 30\%$ above $a/L_{T_i,crit}$), ion and multi-scale simulations produce approximately the same values of driven ion and low-k electron heat flux. Strikingly, near ITG marginality, a nonlinear increase in the high-k ($k_\theta \rho_s > 1.0$), ETG streamer-driven electron heat flux was also observed. Up to 70% of the total Q_e arises from ETG streamers in conditions near marginal, while only limited contributions are found when the low-k turbulence is strongly unstable. As the plasma conditions transition from ETG dominated to ITG dominated, a "U" shaped response of Q_e to increases in a/L_{T_i} occurs in multi-scale simulation. This behavior is in stark contrast to the linear response seen in ion-scale simulation and is a direct
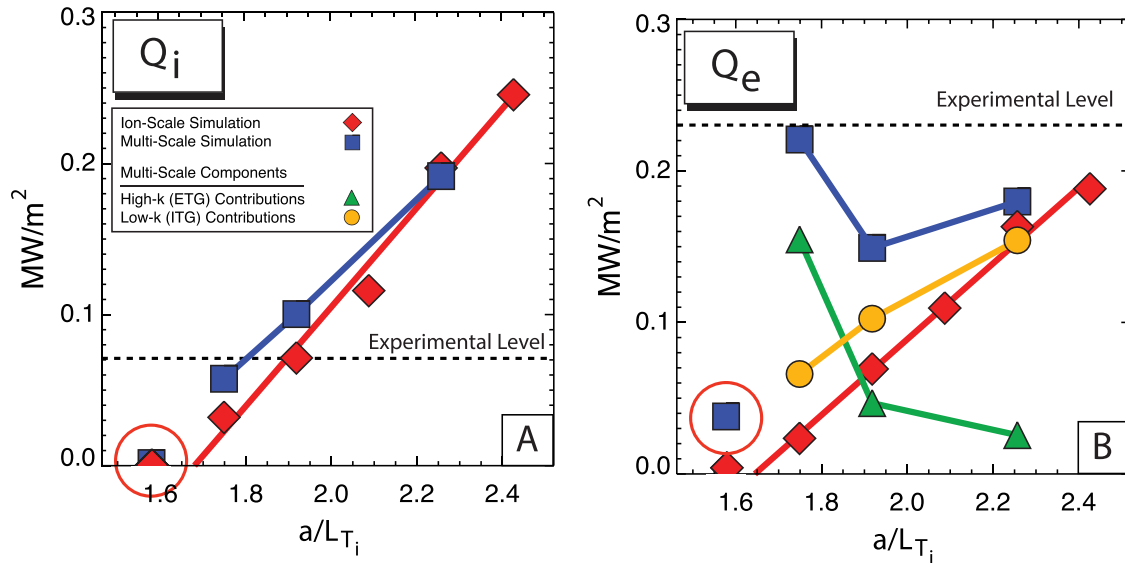
FIG. 1. Multi-scale simulation is compared with ion-scale Q_i (a) and Q_e (b) for 4 values of a/L_{T_i}. The new multi-scale simulation, performed below the ITG critical gradient (low-k turbulence is stable) is circled in both plots.

result of cross-scale interactions of ITG and ETG turbulence. Furthermore, these results highlight the need for simulation of realistic plasma conditions, which often exist with profiles near marginal stability to low-k turbulence.

In addition to probing changes in transport resulting from variations of the ITG drive, (a/L_{T_i}), a second scan, varying the ETG drive, (a/L_{T_e}), was also performed. These results, in addition to a new simulation condition, are plotted in Figure 3. As the ETG drive (a/L_{T_e}) is increased, multi-scale simulation displays an enhancement of low-k ion and electron heat flux (relative to the corresponding ion-scale simulation), indicating the low-k enhancement is seen by both decreasing the ITG drive at fixed ETG drive (as in Figure 1) or by increasing ETG drive at fixed ITG drive. Ion-scale simulation is found to

display little response of simulated Q_e to changes in a/L_{T_e}, implying low electron profile stiffness—qualitatively inconsistent with experiment. In contrast, multi-scale simulation displays a dramatically stronger response of Q_e to a/L_{T_e}, consistent both qualitatively and quantitatively with electron profile stiffness in the experimental discharge studied. Quantitative agreement between values of incremental electron thermal diffusivity, $\chi_{inc} = (1/n_e)dQ_e/d(\nabla T_e)$ obtained from multi-scale simulation, and the heat pulse diffusivity found experimentally[31] was reported in Ref. 26.

The transport highlights from the previous multi-scale simulation work[26] can be summarized as follows:

(1) An increase of the low-k ($k_\theta \rho_s < 1.0$), driven Q_i and Q_e (relative to ion-scale simulation).
(2) Up to 70% of the total Q_e driven by high-k ($k_\theta \rho_s > 1.0$), ETG streamers.
(3) Dramatically different responses of Q_e to changes in ITG (a/L_{T_i}) and ETG (a/L_{T_e}) drive terms when compared to ion-scale simulation.
(4) The ability to simultaneously reproduce experimental Q_i, Q_e, and electron profile stiffness.

B. Cross-scale coupling in multi-scale simulations

In Section III A, the effects of cross-scale coupling on the simulated transport levels were described by comparison of multi-scale simulation with the corresponding ion-scale simulation. In this section, we will outline some of the physical mechanisms responsible for cross-scale coupling in these simulations.

One possible mechanism of coupling between ion and electron-scale turbulence comes in the form of forward and inverse energy cascades that are able to transfer energy between the turbulent scales. To investigate this mechanism in the multi-scale simulations, the energy transfer between three coupled waves existing at distinct spatial scales, where the relationship $k_3 = k_1 + k_2$ (where $k = k_\theta$) exists, was
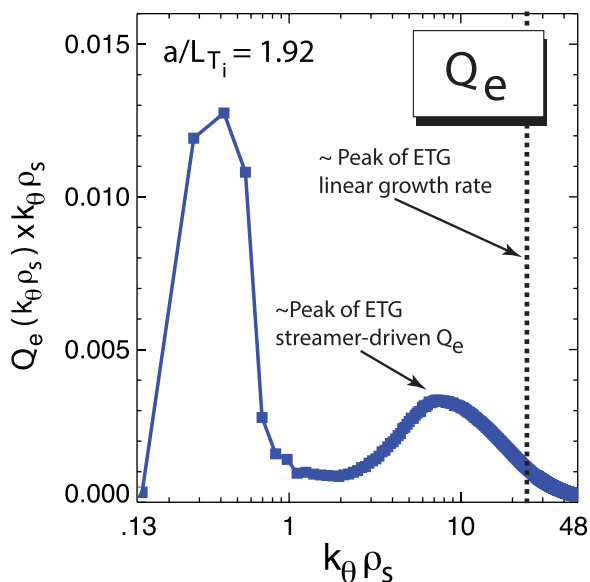

FIG. 2. The electron heat flux spectra for a representative multi-scale simulation ($a/L_{T_i} = 1.92$) is plotted. Note the significant difference between the peak in the ETG linear spectrum with the scale at which streamers are dominant.
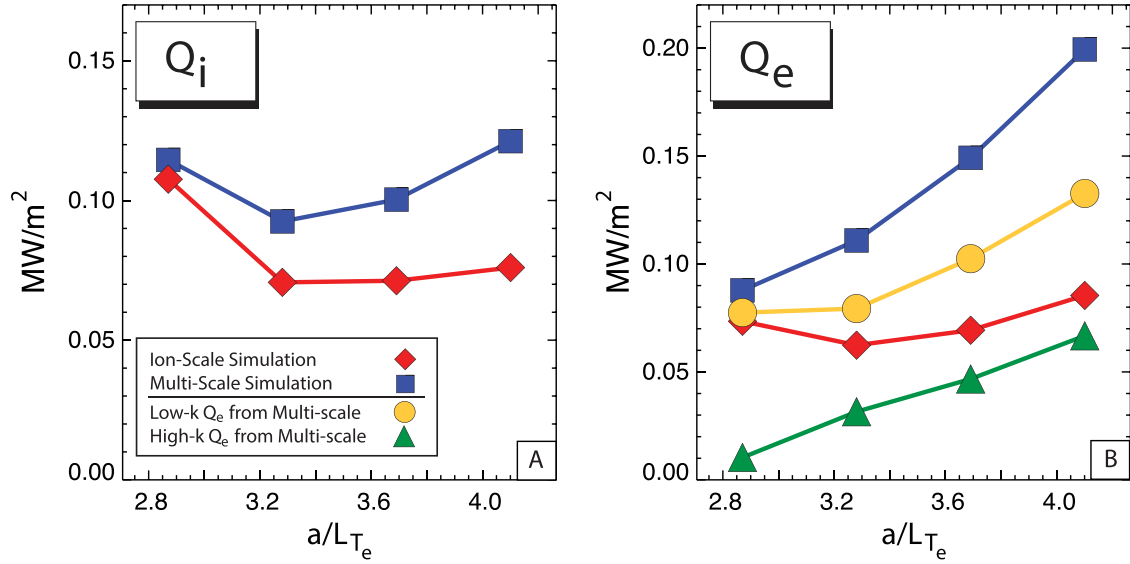
FIG. 3. The ion (a) and electron (b) heat fluxes obtained from ion-scale (red-diamonds) and multi-scale (blue squares) simulation are plotted for a scan of the ETG drive term, a/L_{T_e}. The simulation points are representative of the -1σ, experimental, $+1\sigma$, and $+2\sigma$ values of a/L_{T_e}.

evaluated. Such three wave coupling has been studied in both simulated data[32] as well as experimental fluctuation data[33,34] using higher order spectral analysis. In this analysis, we closely follow the approach outlined in Ref. 32. The total energy transfer function as a function of k_1 and k_3 (with $k_2 = k_3 - k_1$) is written as

$$T(k_3, k_1) = -Re\left\langle \tilde{f}^*(k_3)\tilde{V}_r(k_3 - k_1)\frac{d\tilde{f}(k_1)}{dr}\right\rangle$$
$$- Re\left\langle \tilde{f}^*(k_3)\tilde{V}_\theta(k_3 - k_1)\frac{1}{r}\frac{d\tilde{f}(k_1)}{d\theta}\right\rangle, \quad (1)$$

where $T(k_3, k_1)$ represents the transfer of energy from gradients of a fluctuating field, $\tilde{f}$, that exist as a wavenumber, k_1, to fluctuations existing with a wavenumber, k_3, which are mediated by $E \times B$ velocity fluctuations existing with a wavenumber k_2. The brackets, $\langle\rangle$ in Equation (1) represent a radial and time average of the simulated fluctuations. Negative values (darker colors) of $T(k_3, k_1)$ indicate energy transfer from k_3 to k_1, whereas positive values (lighter colors) represent energy transfer into k_3 from k_1. In order to

most effectively probe the non-adiabatic electron response, analysis of the energy transfer was applied to the simulated electron temperature fluctuations. The results of this analysis performed on conditions in the a/L_{T_i} scan are found in Figure 4.

Examining Figure 4 reveals clear qualitative differences in the energy transfer as the value of a/L_{T_i} is increased (panels (a)–(c)) and the level of ETG streamer-driven heat transport is reduced. Conditions with strong ETG streamers, represented in Figure 4(a), demonstrate the existence of local, and non-local (in wavenumber), inverse cascades focused at wavenumbers associated with ETG streamers. In this condition, the peak of the ETG streamers exists at relatively large scales ($k_\theta\rho_s \sim 3.5$). A local inverse cascade, transferring energy to neighboring k, extends from $k_\theta \sim 1.0$ to 5.0, while the off diagonal features in Figure 4(a) represent non-local inverse energy cascades from ETG wavenumbers ($k_\theta\rho_s \sim [2.0\text{–}7.5]$) extending all the way down to ITG wavenumbers ($k_\theta\rho_s \sim 0.4$). In contrast, the condition studied in Figure 4(c) has strongly unstable ITG turbulence and only small contributions to Q_e from ETG streamers. Although the ETG contributions are
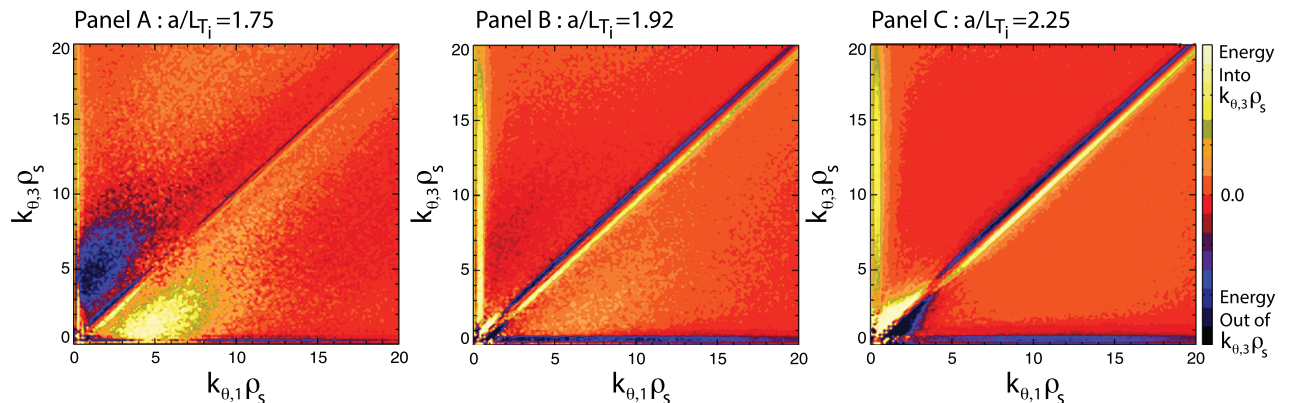

FIG. 4. The energy transfer in simulated electron temperature fluctuations, $T(k_3, k_1)$ is plotted for multi-scale simulations with increasing values of a/L_{T_i} (panels (a)–(c)). Clear changes in energy transfer are observed as the relative importance of ITG and ETG change.

small, they are still present at smaller scales, peaking at approximately $k_\theta\rho_s$ of 10.0–12.0. Local inverse cascades in the ETG wavenumber range are still observed, despite the limited role of streamers in the electron heat transport. The most strikingly different feature is found at low-k, where a local, forward cascade dominates ion-scales and extends up to $k_\theta\rho_s \sim 3.5$, presumably a signature of the strongly unstable low-k turbulence in this condition. All conditions exhibit evidence of a non-local forward energy transfer from ITG wavenumbers to ETG wavenumbers. Consistent with trends observed in the extreme cases, the intermediate condition studied (Figure 4(b)) displays features of both conditions with low and high values of a/L_{T_i}. A combination of forward and inverse (local and nonlocal) cascades exist, consistent with equally important contributions from ITG and ETG turbulence. This analysis demonstrates that ion and electron-scale turbulence interacts via cross-scale energy transfer with the exact type of interaction highly dependent on the mix of low and high-k turbulence.

It was previously reported[26] that multi-scale simulation displays inefficient generation of zonal flow shear. This is quantified by the ratio of long wavelength ($k_\theta = 0$; $k_r\rho_s < 1.0$) zonal flow shear generated for a given amount of power in the finite-n turbulence. To provide the reader with context, results previously reported are shown in Figure 5(a) with new results in Figures 5(b) and 5(c). As shown in Figure 5(a), it was demonstrated that all multi-scale simulations displayed lower values of zonal flow shear efficiency than their corresponding ion-scale simulations and the largest differences occurred when streamers were present and playing a significant role in the overall electron heat transport. Further investigation into this quantity provides more information into the origin of the decreased efficiency. Figures 5(b) and 5(c) plot (in arbitrary units) the numerator (long wavelength zonal flow shear) and denominator (power in the finite-n turbulence) of the zonal flow shear efficiency. For all values of a/L_{T_i}, multi-scale simulation displays very similar values of long wavelength zonal flow shear when compared with the corresponding ion-scale results. In contrast, conditions with strong streamers, existing near the marginal point for ITG ($a/L_{T_i} \sim 1.7$), display significantly higher total power in the finite-n turbulence, resulting

in lower values of zonal flow efficiency. In this analysis, limiting the total power in the multi-scale, finite-n turbulence to include only ion-scales ($k_\theta\rho_s < 1.0$) does not significantly alter the results. The inefficient zonal flow shear generation in multi-scale simulation does not originate from changes to the zonal flow shear itself but instead occurs due to the increased power in the finite-n turbulence. Therefore, in the presence of significant ETG streamers, the total power in the turbulence is able to increase, along with the total low-k driven heat fluxes and fluctuation levels, without generating additional zonal flow shear. Thus, cross-scale coupling of ion and electron-scale turbulence appears to provide a mechanism for increasing low-k heat transport without altering the level of zonal flow shear.

Theory proposed by Holland and Diamond[35] suggests that ITG turbulence, in the form of the self-generated zonal flows as well as the effective shearing due to radial variation of low-k turbulence, may act to regulate ETG in realistic conditions. This theory is qualitatively consistent with the heat fluxes shown in Figure 1 and with results from reduced mass, multi-scale simulation.[19,23] As the drive for the low-k turbulence is increased and the role of ITG becomes more dominant, the level of high-k driven electron heat flux is found to decrease. To investigate this interaction more completely, we follow roughly the approach outlined by Candy *et al.*,[19] to evaluate the effective shearing due to zonal flows and low-k turbulence. Define the shear as a function of k_r and k_θ as

$$S(k_\theta, k_r) = \sqrt{(\rho_s c_s)^2 \left| (k_\theta^2 + k_r^2) \frac{e\tilde{\phi}}{T} \right|^2} \sim \sqrt{\left| \frac{\partial v_x}{\partial y} + \frac{\partial v_y}{\partial x} \right|^2}.$$

(2)

For this analysis, the components $k_\theta\rho_s$ and $k_r\rho_s$ values that are less than 1.0 were considered. The effective RMS long wavelength shearing rate is therefore given by

$$\omega_{rms} = \sqrt{\langle (S(k_\theta\rho_s \leq 1.0, k_r\rho_s < 1.0)^2) \rangle},$$

(3)

where the brackets, $\langle\rangle$ denote an average. We have chosen to include only long wavelength, $k_\theta\rho_s < 1.0$; $k_r\rho_s < 1.0$
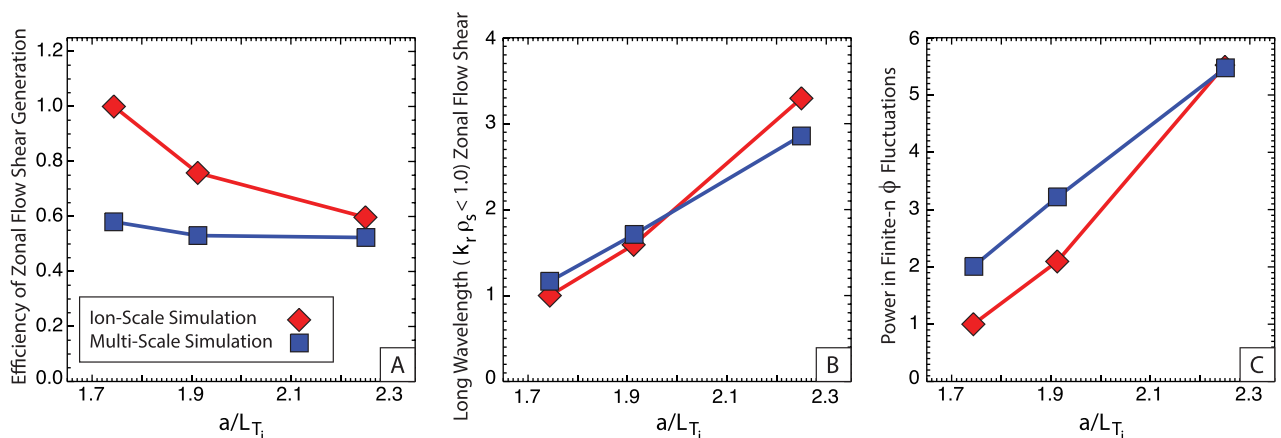

FIG. 5. The zonal flow efficiency (a) long wavelength ($k_r\rho_s < 1.0$) zonal flow shear (b) and power in the finite-n turbulence (c) are plotted for ion and multi-scale simulations at different values of a/L_{T_i}.
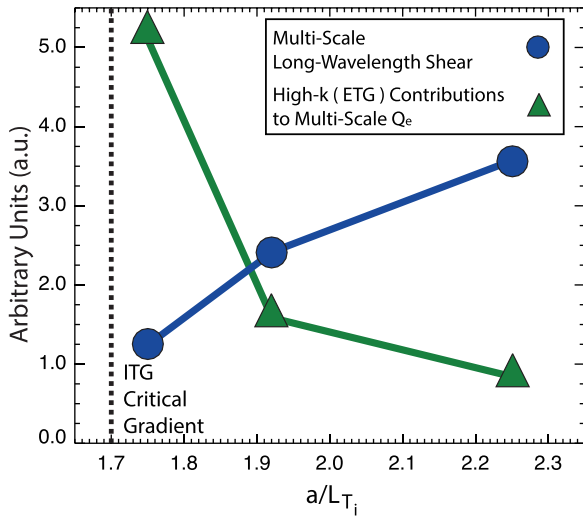
FIG. 6. For 3 multi-scale simulations, spanning values of a/L_{T_i}, the high-k contributions to the electron heat flux and the total shear due to long wavelength ($k_r \rho_s < 1.0$), low-k turbulence is plotted in arbitrary units.

components, as the longer wavelength radial components are more effective at shearing apart the large turbulent structures primarily responsible for heat and particle transport and we are interested in the shearing effect related to low-k_θ (ITG) turbulence. In Figure 6, the high-k contributions to the multi-scale electron heat flux obtained from simulations with 3 values of a/L_{T_i} are plotted in arbitrary units. Overplotted is the shear due to long wavelength components of zonal + finite-n turbulence, also in arbitrary units. As noted above, the total high-k driven Q_e significantly decreases with a/L_{T_i} and this decrease is correlated with an increase in the effective shearing of the low-k turbulence, suggestive of long wavelength suppression of the ETG. The derived shearing rates are well below ($\sim$1/60th) the peak linear growth rate for the ETG. However, when compared with the turbulence decorrelation rate evaluated using only the high-k_θ potential fluctuations, the effective shearing rates are more comparable ($\omega_{rms}/\gamma_{decorrelation} \sim 0.1$–0.33) and the ratio of shearing rate to decorrelation rate is found to increase with a/L_{T_i}. Therefore, it is plausible that the effective low-k shearing is playing a non-negligible role in ETG saturation. We note that if high-k_r components are included in the calculation, the effective shearing rates reach values of approximately 50% of the high-k decorrelation rate. However, previous work suggests such components exist at high frequencies[36] and are therefore ineffective at regulating turbulence. The exact mechanism of the ETG saturation is still an open question and has been investigated in recent work based on these multi-scale simulations.[37]

C. Multi-scale simulation in conditions with suppressed ion-scale turbulence

As described in Section III B, conditions with significant ETG streamers were found to exhibit a clear increase in the low-k driven heat fluxes (ion and electron) relative to ion-scale only simulation. In an attempt to understand cross-scale coupling in conditions where ion-scale turbulence is effectively suppressed, we performed an additional

simulation at an a/L_{T_i} value of approximately 1.6, below the ITG critical gradient determined by ion-scale simulation (see Figure 1). It is important to note that this condition was simulated for approximately 250 a/c_s and the quoted quantities were obtained from substantially shorter time averages ($\sim$40$a/c_s \leftrightarrow$ 2400 $a/v_{th,e}$) than the other multi-scale cases. However, as ion-scale turbulence is absent in this condition, this multi-scale simulation is effectively an electron-scale simulation at extremely large box size. As a result, the dynamics of interest exist on the electron-scale turbulence timescales and the heat fluxes are very steady over the averaging period. The results from this new simulation point to some interesting aspects of the physics of cross-scale coupling. Although conditions with marginally stable ITG turbulence demonstrate a clear enhancement of the low-k ion and electron heat flux, no such increase is observed in this simulation condition. Multi-scale simulation displays effectively no heat transport arising from the ion-scale. This suggests that the presence of unstable ion-scale turbulence is a necessary condition for multi-scale simulation to display substantially enhanced heat flux from the low-k. More specifically, the physical processes associated with the low-k enhancement do not appear to generate the turbulence itself, only enhance the existing turbulence. Furthermore, the electron heat flux driven in multi-scale simulation of this condition ($a/L_{T_i} \sim 1.6$) is small ($\sim$1/6th) compared with the electron heat flux driven at marginal conditions ($a/L_{T_i} \sim 1.7$). This result suggests that the presence of the low-k turbulence is needed to allow the high-k turbulence (ETG streamers) to saturate at higher levels, and thus drive more heat transport. Since ion-scale turbulence is absent in this condition, we performed the corresponding electron-scale simulation (64 toroidal modes up to $k_\theta \rho_s = 48.0$, $2\rho_e$ grid spacing, $16 \times 8\rho_s$ box sizes ($2\rho_s$ buffers)—otherwise identical to multi-scale simulations) for this plasma condition. Consistent with naive expectations for conditions with suppressed ion-scale turbulence, the results from electron-scale simulation yield nearly identical values of electron heat flux, all of which arise from high-k contributions.

D. Multi-scale simulation and the origin of electron profile stiffness

In order to better understand the response of multi-scale heat fluxes to changes in the ETG drive term, an additional multi-scale simulation, with a value of $a/L_{T_e} \sim 4.1$, or $+2\sigma$ (25%) above its experimental value, was performed (see Figure 3). The results from this new simulation elucidate some of the key observations from multi-scale simulation. Extrapolating the high-k driven heat flux (green triangles) to the x-axis, and defining this point as the nonlinear ETG critical gradient, results in an $a/L_{T_{e,crit}}$ of approximately 2.65. Interestingly, this value is significantly upshifted from the linear critical gradient, which is found (not shown) to occur at a value of approximately $a/L_{T_e} = 1.4$. This upshift is likely related to the effective shearing of ETG turbulence due to the long wavelength turbulence (zonal components and finite-n). We note that the total Q_e obtained from multi-scale simulation displays a slightly nonlinear trend with

increases in a/L_{T_e}. Such a nonlinear increase may explain some electron profile stiffness observations reported previously,[38–40] where similar nonlinear response is present. Looking at the individual low and high-k contributions to the total electron heat flux, the origin of this response is clearly seen. For the range of a/L_{T_e} scanned, the increase in high-k, Q_e contributions appears approximately linear, consistent with expectations based on linear growth rates. However, as the value of a/L_{T_e} is increased, the enhancement of the low-k electron (and ion) heat fluxes also increases, leading to a total heat flux that increases nonlinearly with a/L_{T_e}. This response is a likely origin of the extremely stiff electron temperature profiles observed experimentally.[41]

Detailed experiments were recently performed on DIII-D to probe electron profile stiffness in L-mode plasma conditions.[38] These experiments utilized varying levels of Electron Cyclotron Heating (ECH) to systematically vary the local value of a/L_{T_e} and study the changes the experimental electron heat flux. Hillesheim *et al.* reported the observation of a nonlinear critical gradient in the electron temperature fluctuations which was concluded to represent the critical gradient for low-k, Trapped Electron Mode (TEM) turbulence.[40,42] This conclusion was based largely on linear stability analysis and fluctuation measurements (Correlation Electron Cyclotron Emission (CECE): $\tilde{T}_e/T_e$ measurement and Beam Emission Spectroscopy (BES): $\tilde{n}_e/n_e$ measurement) which demonstrate a weak response of long wavelength density fluctuations to a/L_{T_e} accompanied by strong changes in measured T_e fluctuations. The possible role of ETG was not investigated. Subsequent nonlinear gyrokinetic modeling, based on a subset of the original discharges, revealed that at high values of a/L_{T_e}, GYRO systematically underestimates the electron heat flux, CECE fluctuation level, and electron profile stiffness using ion-scale (ITG/TEM) simulation.[39]

To connect with the DIII-D experiments and the long wavelength CECE and BES turbulence measurements, the RMS fluctuation level arising from the $k_\theta\rho_s \lesssim 0.4$ was evaluated for all points in the a/L_{T_e} scan. Although a synthetic diagnostic is needed to make quantitative comparison with these turbulence measurements, examining the fluctuation levels changes in the $k_\theta\rho_s \lesssim 0.4$ range should allow for qualitative comparison. Plots of the relative electron density and temperature fluctuation levels (in %) for ion and multi-scale simulations are plotted in Figure 7. Resulting from the enhanced low-k transport, the multi-scale fluctuation levels exceed the ion-scale results at values of a/L_{T_e} where ETG is significantly unstable. Figures 3 and 7 demonstrate results that are qualitatively consistent with the experimental and modeling observations reported in Refs. 39, 40, and 42. Namely, as the drive for ETG increases, only a weak response of density fluctuations (12%) is observed to occur with a strong increase in temperature fluctuations (73%), qualitatively identical to the results reported by Hillesheim. Furthermore, the ion-scale (ITG/TEM) simulation of the DIII-D discharges[39] produces systemically lower values of Q_e and is unable to reproduce experimental levels of profile stiffness at high values of a/L_{T_e}, identical to the results from the low-power discharge (demonstrated
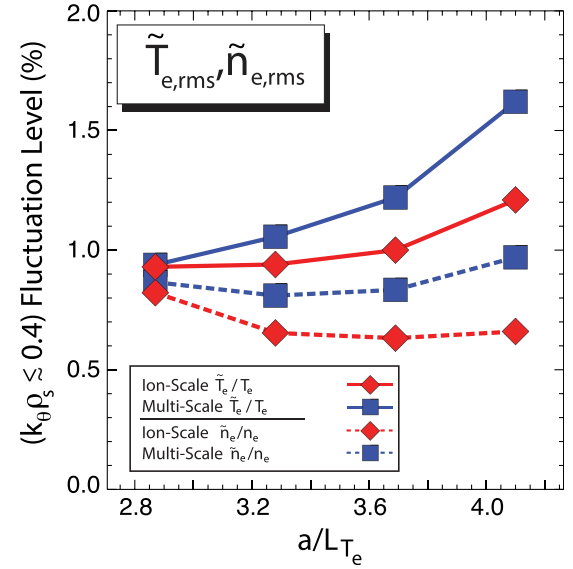

FIG. 7. The RMS relative fluctuation levels of electron density and temperature arising from $k_\theta\rho_s \lesssim 0.4$ are plotted for ion-scale and multi-scale simulations for all points in the a/L_{T_e} scan. Notice the much stronger increase of the electron temperature fluctuation level relative to the modest increase in density fluctuations as a/L_{T_e} is scanned.

in Figure 3). Given the similarity of the conditions reported here with those reported from DIII-D, the multi-scale results suggest that the critical gradient, electron profile stiffness, and fluctuation measurements reported by Hillesheim *et al.* may actually be more indicative of the role of ETG turbulence than of low-k TEM as reported. This statement does not imply that low-k TEM is not present in the experimental conditions, only that the cross-scale coupling of ETG with long wavelength turbulence (via enhancement of low-k turbulence) is possibly a dominant factor in the critical gradient behavior observed. Future work will seek to directly confirm this statement by performing additional simulations.

IV. MULTI-SCALE SIMULATION OF A HIGH POWER, L-MODE DISCHARGE

To explore the role of cross-scale turbulence coupling in a different plasma condition and the generality of the results reported from the low-power discharge, multi-scale simulation was performed on a high-power (3.5 MW ICRH), L-mode discharge at r/a = 0.6.

A single, multi-scale scale simulation was performed on this discharge, utilizing the heat flux-matched gradients obtained from ion-scale simulation. Using the plotting style proposed by Görler and Jenko,[20] the heat flux spectra for both ion and multi-scale simulation of this discharge are presented in Figure 8. Some notable features are present in this figure. As with the low-power discharge,[22] effectively all ion heat flux arises from scales with $k_\theta\rho_s < 1.0$, while significant electron heat flux is driven at ETG-relevant scales ($k_\theta\rho_s > 1.0$). In fact, approximately 42% of the total electron heat flux arises from $k_\theta\rho_s > 1.0$, indicating an important role of ETG in this particular discharge. A clear enhancement of the low-k driven heat flux is found in the ion and electron
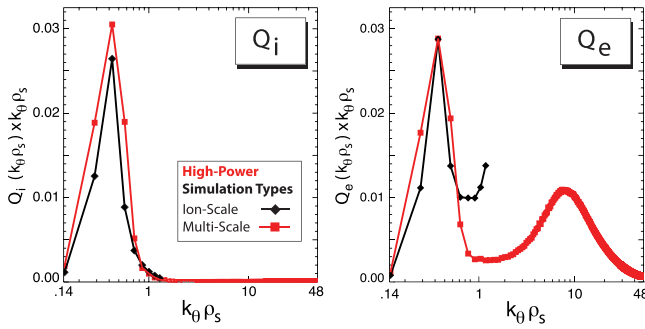
FIG. 8. The heat flux spectra, $Q_i \times k_\theta \rho_s$ (a) and $Q_e \times k_\theta \rho_s$ (b), are plotted for both ion and multi-scale simulation of the high-power discharge. The plot style proposed by Gorler *et al.* is used such that the area under the curve is indicative of the heat flux driven at each scale.

channels, consistent with the findings from the low-power discharge.

The magnitude of the low-k enhancement and the importance of ETG turbulence in the multi-scale simulation are perhaps best displayed in Figure 9, where the total ion and electron heat fluxes obtained from ion and multi-scale simulation are plotted.

Ion-scale simulation of this discharge is able to reproduce both experimental ion and electron heat fluxes within diagnosed experimental uncertainties. It was previously speculated that this result implied that only marginal increases in the electron heat flux would be obtained from the inclusion of high-k contributions.[28] However, multi-scale simulation actually displays an increase in both the ion ($\sim$0.06 MW/m^2 or 40%) and electron ($\sim$0.13 MW/m^2 or 70%) heat fluxes. The increase in the ion heat flux results in a simulation that no longer matches the experimental ion heat flux levels, while the electron heat flux still remains in agreement within uncertainties. In attempt to resolve this discrepancy, an additional multi-scale simulation was attempted with only a 3% reduction in a/L_{T_i}. Unfortunately, the transport in this condition was found to be extremely stiff. A 3% reduction resulted in ion heat fluxes that decayed in time and approximately constant or slightly increased electron heat flux levels, indicating the ITG turbulence is stable with only a small reduction in a/L_{T_i}. As computing resources are limited, we chose not to run this condition to completion.

However, this result suggests that experimental ion and electron heat fluxes can likely be matched by multi-scale simulation with less than a 3% change in the value of a/L_{T_i}. Any such change would be well within experimental uncertainties. The results from simulation of the high-power discharge underscore the need for additional modeling constraints when validating the gyrokinetic model. Within experimental uncertainties, both ion-scale and multi-scale simulations can likely reproduce ion and electron heat fluxes simultaneously but would display fundamentally different turbulence characteristics.

The energy transfer analysis described above was also performed on the simulated electron temperature fluctuations from the high-power discharge. The results of this analysis are qualitatively consistent with the results from the low-power discharge. The strongly unstable low-k turbulence results in a local and nonlocal forward cascade at long wavelengths, while local and non-local inverse cascades are observed in the ETG wavenumber range ($k_\theta \rho_s \sim 8.0$) for this discharge. These results are similar to those reported in Figure 4(b).

V. SIGNATURES OF ETG TURBULENCE AND CROSS-SCALE COUPLING IN EXPERIMENTAL CONDITIONS

The previous sections outlined the comparison of both ion and multi-scale simulation with experimental heat fluxes, clearly demonstrating the need for additional constraints for gyrokinetic model validation. In this section, we present signatures of ETG turbulence demonstrated in the multi-scale simulations, which may be accessible to current diagnostics. Such measurements could provide a more direct confirmation of ETG turbulence and a more rigorous set of comparisons for gyrokinetic model validation. Most of the analysis presented here will focus on the a/L_{T_i} scan in the low power discharge. These conditions are chosen to best demonstrate the clear differences in conditions with "weak" and "strong" streamers.

The power spectrum of the density fluctuations, averaged in radius and time, is plotted for 3 values of a/L_{T_i} in Figure 10. Clear differences in the density fluctuation spectrum are observed as the importance of ETG streamers decreases (with increasing values of a/L_{T_i}). In addition to the low-k peak ($k_\theta \rho_s = 0.3$–0.4.) resulting from the ITG turbulence, conditions with strongly unstable streamers, ($a/L_{T_i} = 1.75$) exhibit a clear secondary peak in the density fluctuation spectrum, occurring at approximately $k_\theta \rho_s = 3.5$. As a/L_{T_i} is increased, the secondary peak shifts to higher values of k_θ, eventually manifesting itself as a flattening in the spectrum. We note that the observation of a secondary flattening in the density fluctuations is in qualitative agreement with multi-scale simulations performed by Görler and Jenko[43] using variations of CYCLONE base case parameters. To connect to both previous work[14,43] and fluid theories of turbulence, we have fit portions of the spectrum to power laws with the functional form $|n_e|^2 \propto c_1 k_\theta^{-x}$ where the value of c_1 is a constant and x is referred to as the spectral index. Such power-law fits to the spectra may also provide an useful comparison with fluctuation measurements, as clear trends are found with changes in a/L_{T_i} both in the intermediate k
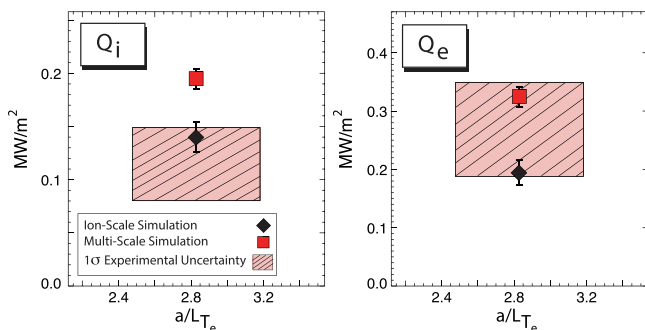

FIG. 9. The heat fluxes from both ion and multi-scale simulation of the high-power discharge are compared with the experimental levels. A clear enhancement of the ion heat flux is seen in the multi-scale simulation.
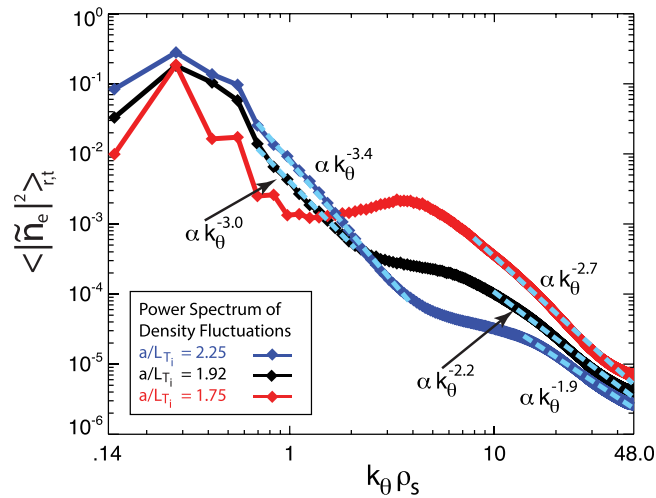
FIG. 10. The power spectrum of the density fluctuations obtained from simulations with different values of a/L_{T_i} are plotted. Conditions with high values a/L_{T_i} exhibit weak streamers, while conditions at low a/L_{T_i} are ETG streamer dominated as demonstrated by the high-k peak in the spectrum. Fits to the spectra of the form $\propto c_1 k_\theta^{-x}$ are also plotted.

range (between low and high-k peaks) and in the high-k range (above the secondary peak or flattening). In the intermediate-k range ($k_\theta \rho_s \sim 1.0$–4.0), a clear decrease in the spectra index occurs with a/L_{T_i}, while the spectral index in the high-k range shows the opposite trend. The results of this analysis have clear importance to the comparison of simulation with experiment. Currently operating systems such as the Doppler Backscattering (DBS)[44] and the Phase Contrast Imaging (PCI) systems have the ability to observe density fluctuations in the intermediate-k range $k_\theta \rho_s \sim 1$–3. These results indicate such measurements could play a crucial role in validation of multi-scale models and may capture signatures of strongly unstable ETG. Conditions with strongly unstable ETG streamers may exhibit a flattening, or slight increase in the density fluctuation spectrum in the detectable k-range that would manifest itself as a decrease in the spectral index. Such a change in the fluctuation spectrum would not be captured in ion-scale simulation or in multi-scale simulation with only weakly unstable ETG turbulence, making it a strong constraint for model validation.

Contours of the electron density fluctuation spectra are plotted in Figure 11 for conditions with weak (a) and strong (b) ETG streamers. These plots demonstrate some interesting features. As expected, the presence of strong ETG streamers results in a highly anisotropic fluctuation spectrum at nearly all scales. In contrast, the condition with weak ETG streamers (Figure 11(a)) displays an approximately isotropic fluctuation spectrum in the low-k range ($k\rho_s < 1.0$) and a clearly anisotropic spectrum at higher-k. This result indicates that conditions even with weak ETG streamers exhibit an anisotropic density fluctuation spectrum. This is in contrast with assumptions previously used to interpret some experimental measurements[45] and with previous results obtained from reduced mass, multi-scale simulation.[18,19] Anisotropy of the fluctuations has important implications for the detection of ETG features experimentally as current experimental
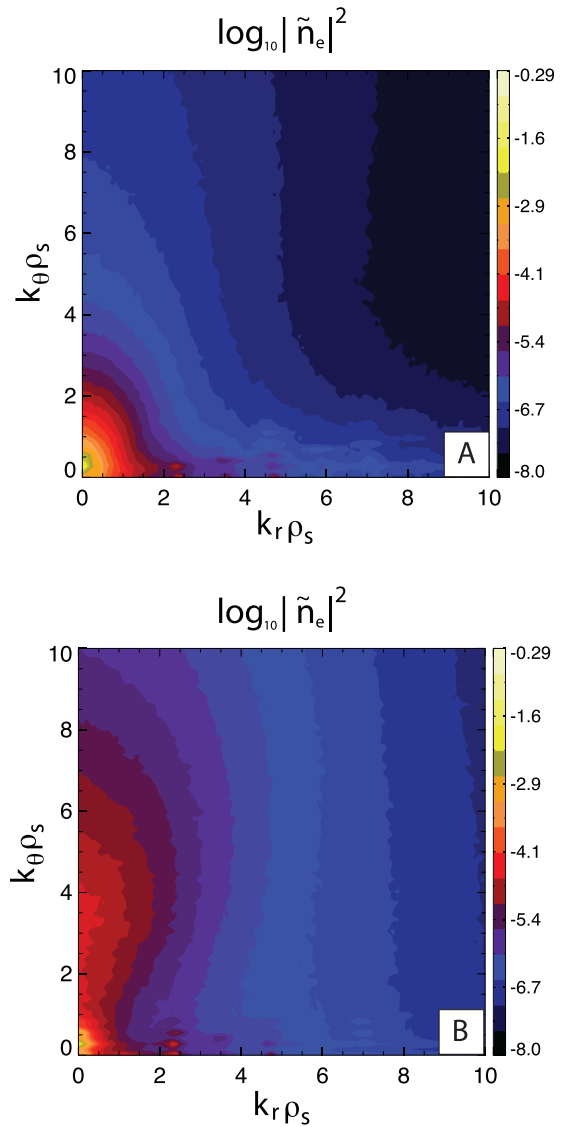

FIG. 11. Contours of the electron density spectra in the range [0.0–10.0] are plotted versus $k_r \rho_s$ and $k_\theta \rho_s$ on the x and y-axes, respectively. Results from multi-scale simulation for conditions with weak [strong] ETG streamers are plotted in panel (a) [(b)]. At high-k, a clear anisotropy of the fluctuations is found in conditions with both weak and strong ETG streamers.

evidence for ETG fluctuations has been predominantly obtained from scattering systems[45–47] designed to probe high k_r while measuring relatively low values of k_θ.[48,49] In general, such measurements have been interpreted using ETG linear growth rates. However, the nonlinear results shown here demonstrate that although the linear ETG growth rate peaks at approximately $k_\theta \rho_s \sim 24.0$ (Figure 12), the peak in the fluctuations in nonlinear simulations tend to exist at much larger scales ($k_\theta \rho_s \sim 3$–12). Additionally, it is demonstrated that changes in the fluctuation spectrum at ETG wavenumbers can be independent of changes in the ETG drive term (as demonstrated in Figures 12 and 11: where only the ITG drive is scanned). Therefore, interpretation of scattering measurements using ETG linear stability may not be a valid in many plasma conditions, and a more rigorous comparison of the fluctuation spectrum obtained from nonlinear simulation, perhaps even multi-scale simulation, is likely required.
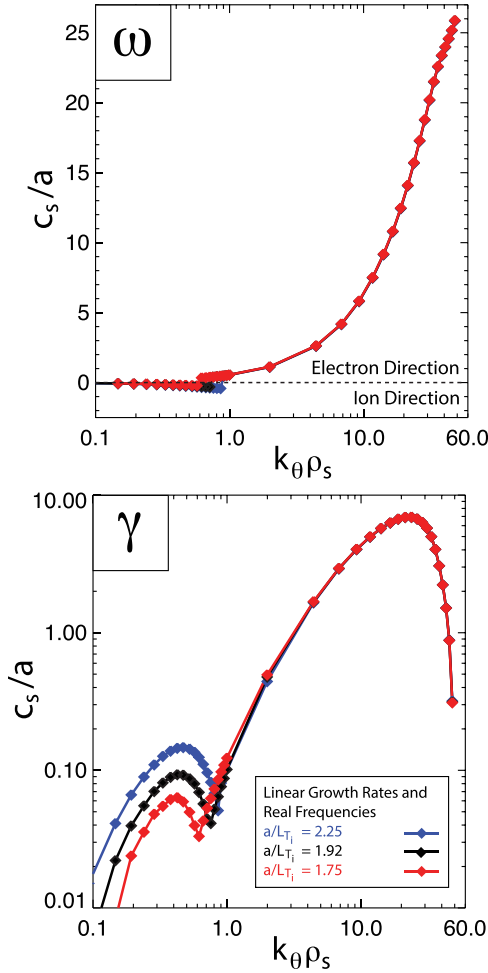
FIG. 12. The real frequencies (top) and linear growth rates (bottom) are plotted for the 3 conditions simulated in the scan of a/L_{T_i}.

VI. INSIGHTS INTO CROSS-SCALE COUPLING FROM LINEAR PHYSICS

The resources required to perform realistic mass, multi-scale simulation and the demonstration that cross-scale coupling plays an important role in some regions of parameter space, motivates a search for simple models or "rules of thumb." Such rules could allow for rough predictions of when cross-scale coupling plays an important role, and therefore, when multi-scale simulation might be required. In this section, we attempt to provide some insight into the importance of cross-scale coupling based on linear growth rates. However, it is important to note that these results are based on a limited region of parameter space and only a handful of simulations and therefore the generality of these results are obviously unknown. These observations should be considered a starting point, to be built upon by future multi-scale simulation results.

We begin by quantifying the relative "strength" of ETG and ITG by the linear growth rates. Using ∼40 point scans from approximately $k_\theta \rho_s = 0.1$ to 48.0 for each condition simulated (low and high power), the maximum linear growth rate in the ITG-relevant range, defined to be $k_\theta \rho_s = [0.25–0.75]$ and the maximum linear growth rate in the range $k_\theta \rho_s = [2.0–48.0]$ (see Figure 12) is evaluated. Generally, the maximum low and high-k linear growth rates occur approximately in the middle of the defined ranges for the conditions simulated. We will refer to the low and high-k growth rates now as values of γ_{low-k} and γ_{high-k}, respectively, throughout the remainder of the paper.

Three transport phenomena have been identified as signatures of multi-scale simulations that cannot be captured by a standard ion-scale simulation: (1) Heat flux driven directly by high-k turbulence, (2) increases in low-k driven electron heat flux, and (3) Increases in low-k driven ion heat flux. These quantities are plotted in Figure 13 panels (a)–(c). In Figure 13(a), we plot the gyro-Bohm normalized (where $Q_{gB} = n_e c_s T_e (\rho_s/a)^2$), high-k electron heat flux ($k_\theta \rho_s > 1.0$) versus the ratio of $\gamma_{high-k}/\gamma_{low-k}$ extracted from linear simulations. Blue points indicate multi-scale simulations of the low power discharge, and red points indicate the simulation of the high-power discharge. If plotted in unnormalized units (MW/m^2), the high-power discharge would represent a clear outlier on this plot. However, due to the much larger gyro-Bohm unit (due to the higher temperature), the high-power discharge falls along the curve of the low-power simulations. Following with what may have been a naive expectation, a very clear increase in the high-k driven electron heat flux
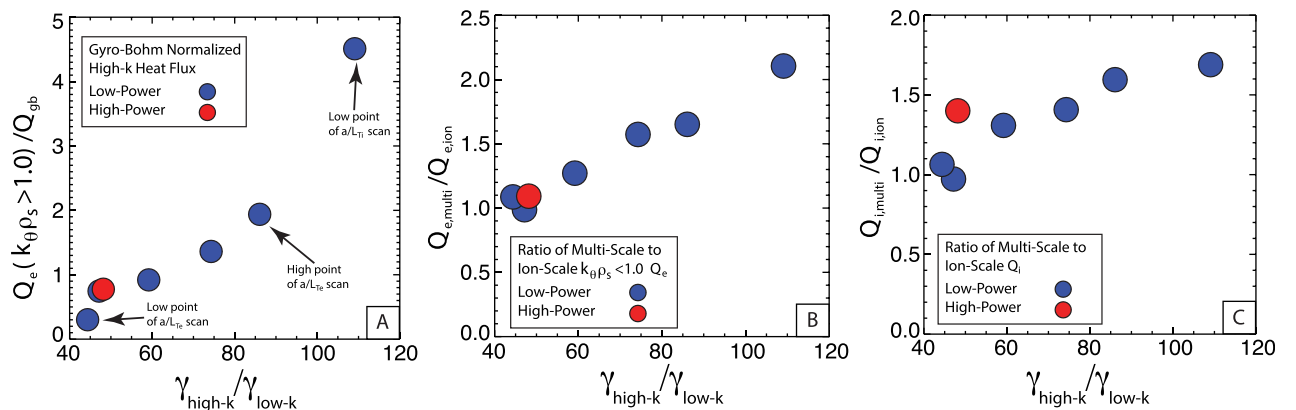

FIG. 13. Results from multi-scale simulations are plotted versus the ratio $\gamma_{high-k}/\gamma_{low-k}$. Panel (a) plots the gyro-Bohm normalized high-k ($k_\theta \rho_s > 1.0$) driven electron heat flux. Panel (b) plots the ratio of the low-k ($k_\theta \rho_s < 1.0$) driven electron heat flux from multi-scale simulation to the low-k driven electron heat flux from ion-scale simulation, and panel (c) plots ratio of the multi-scale ion heat flux to ion-scale ion heat flux.

with the ratio $\gamma_{high-k}/\gamma_{low-k}$ is observed in this plot. The response of the high-k heat flux to the growth rate ratio appears to be nonlinear for the cases considered.

In an attempt to quantify the increase in the low-k heat fluxes obtained from multi-scale simulation (relative to ion-scale simulation), Figure 13(b) plots the ratio of the low-k ($k_\theta\rho_s < 1.0$) multi-scale to ion-scale electron heat fluxes, while Figure 13(c) plots the ratio of the multi-scale to ion-scale ion heat flux versus the ratio $\gamma_{high-k}/\gamma_{low-k}$. Although there is some variation with the points, both plots show approximately linear increases in the heat flux ratio with increasing linear growth rate ratio. These results suggest that a simple rule of thumb to predict the importance of multi-scale effects may be possible. For conditions studied, it appears as though the effects of cross-scale coupling diminish at a ratio $\gamma_{high-k}/\gamma_{low-k} \lesssim 40.0$. However, these linear results should only be viewed as a first attempt at a simple rule of thumb as it is likely that future multi-scale scale simulations will demonstrate a dependence on a number of quantities that were not investigated here (i.e., $\hat{s}, q, \gamma_{E\times B}$, etc.). Further investigation is left for future work.

VII. SUMMARY AND CONCLUSIONS

Results from 8 realistic mass, multi-scale simulations were presented in this paper. These simulations were performed on two Alcator C-Mod, L-mode plasma conditions, operated at different levels of ICRH input power. It was demonstrated that multi-scale simulation can display significant high-k electron heat flux as well as enhance low-k contributions to both the electron and ion heat flux (relative to ion-scale simulation), resolving some discrepancies between ion-scale simulation and experimental electron heat flux and electron profile stiffness. The mechanisms of cross-scale coupling were discussed. Electron and ion-scale turbulence are found to interact through a variety of energy cascades which vary with the relative strength of low-k and high-k instabilities, and the presence of ETG in multi-scale simulation appears to break the relationship between total power in finite-n turbulence and zonal flow shear generation found in ion-scale simulation. It was demonstrated that the effective shearing due to long wavelength turbulence likely plays a role in the suppression of ETG driven heat transport.

The effects of cross-scale coupling play an important role in the interpretation of simulated and experimental heat fluxes as well as fluctuation measurements. The enhancement of low-k heat fluxes (Figures 1 and 3) and turbulence levels (Figure 7) demonstrates that independent electron and ion-scale simulations cannot be simply added to obtain the results of multi-scale simulation, as these phenomena cannot be captured by any single-scale simulation. Furthermore, cross-scale interactions strongly call into question the use of linear stability analysis for the interpretation of fluctuation measurements. The assumption that changes in fluctuations are tracked by changes in linear instabilities at the measured scale (instabilities existing in the diagnostic k-range) is inherently flawed for conditions exhibiting cross-scale coupling, as changes in the stability of low-k turbulence are found to greatly effect high-k turbulence (Figure 1) and vice versa (Figures 3 and 7).

TABLE I. A list of parameters, definitions, and values used as simulation inputs for the high power discharge. For more details on definitions see Ref. 50 and for low-power simulation inputs, the reader is referred to Ref. 26.

r/a	Normalized midplane minor radius	0.60
a (m)	Minor radius	0.22
$n_e (10^{20}\,\text{m}^{-3})$	Electron density	1.07
T_e (keV)	Electron temperature	1.98
a/L_n	Normalized density gradient scale length	1.11
a/L_{T_e}	Normalized electron temperature gradient scale length	2.83
a/L_{T_i}	Normalized ion temperature gradient scale length	1.47
a/L_{T_B}	Normalized impurity temperature gradient scale length	1.47
$T_i/T_e = T_B/T_e$	Ratio of ion temperature to electron temperature	0.81
n_D/n_e	Ratio of deuterium to electron density	0.90
n_B/n_e	Ratio of impurity to electron density	0.02
Z_{eff}	Effective ion charge	2.75
$\nu_{ei} (a/c_s)$	Electron-ion collision frequency	0.052
$R_0(r)/a$	Aspect ratio	3.12
$\Delta = dR_0(r)/dr$	Shrafronov shift	−0.12
q	Safety factor	1.61
$\hat{s} = r\,dln(q)/dr$	Magnetic shear	1.36
κ	Plasma elongation	1.25
$s_\kappa = r\,dln(\kappa)/dr$	Elongation shear	0.12
δ	Plasma triangularity	0.12
$s_\delta = r\,d\delta/dr$	Triangularity shear	0.21
$M_\phi (a/c_s)$	Toroidal Mach number	0.12
$\gamma_{ExB} (a/c_s)$	$E\times B$ shearing rate	0.04
$\gamma_p (a/c_s)$	Rotation shearing rate	0.29
$\rho^* = \rho_s/a$	Ratio of sound speed gyroradius to minor radius	0.004
a/c_s (μs)	Ratio of minor radius to sound speed	0.71

An initial attempt to derive a "rule of thumb" based on linear growth rates was presented with the objective of roughly predicting the importance of multi-scale effects. Clear trends of high-k driven heat flux and enhanced low-k turbulence with the relative values of ETG and ITG linear growth rates were demonstrated, suggesting that development of a simple rule may be possible. Future investigations into this possibility should be pursued as additional multi-scale simulations are completed.

[1]D. W. Ross and W. Dorland, "Comparing simulation of plasma turbulence with experiment. II. Gyrokinetic simulations," Phys. Plasmas **9**(12), 5031–5035 (2002).

[2]A. E. White, L. Schmitz, G. R. McKee, C. Holland, W. A. Peebles, T. A. Carter, M. W. Shafer, M. E. Austin, K. H. Burrell, J. Candy, J. C. DeBoo, E. J. Doyle, M. A. Makowski, R. Prater, T. L. Rhodes, G. M. Staebler, G. R. Tynan, R. E. Waltz, and G. Wang, "Measurements of core electron temperature and density fluctuations in DIII-D and comparison to nonlinear gyrokinetic simulations," Phys. Plasmas **15**(5), 056116 (2008).

[3]A. Casati, T. Gerbaud, P. Hennequin, C. Bourdelle, J. Candy, F. Clairet, X. Garbet, V. Grandgirard, Ö. D. Gürcan, S. Heuraux, G. T. Hoang, C. Honoré, F. Imbeaux, R. Sabot, Y. Sarazin, L. Vermare, and R. E. Waltz, "Turbulence in the tore supra tokamak: Measurements and validation of nonlinear simulations," Phys. Rev. Lett. **102**, 165005 (2009).

[4]C. Holland, A. E. White, G. R. McKee, M. W. Shafer, J. Candy, R. E. Waltz, L. Schmitz, and G. R. Tynan, "Implementation and application of two synthetic diagnostics for validating simulations of core tokamak turbulence," Phys. Plasmas **16**(5), 052301 (2009).

[5]A. E. White, W. A. Peebles, T. L. Rhodes, C. H. Holland, G. Wang, L. Schmitz, T. A. Carter, J. C. Hillesheim, E. J. Doyle, L. Zeng, G. R. McKee, G. M. Staebler, R. E. Waltz, J. C. DeBoo, C. C. Petty, and K. H. Burrell, "Measurements of the cross-phase angle between density and electron temperature fluctuations and comparison with gyrokinetic simulations," Phys. Plasmas **17**(5), 056103 (2010).

[6]J. C. DeBoo, C. Holland, T. L. Rhodes, L. Schmitz, G. Wang, A. E. White, M. E. Austin, E. J. Doyle, J. Hillesheim, W. A. Peebles, C. C. Petty, Z. Yan, and L. Zeng, "Probing plasma turbulence by modulating the electron temperature gradient," Phys. Plasmas **17**(5), 056105 (2010).

[7]N. T. Howard, M. Greenwald, D. R. Mikkelsen, M. L. Reinke, A. E. White, D. Ernst, Y. Podpaly, and J. Candy, "Quantitative comparison of experimental impurity transport with nonlinear gyrokinetic simulation in an Alcator C-Mod L-mode plasma," Nucl. Fusion **52**(6), 063002 (2012).

[8]W. Guttenfelder, J. L. Peterson, J. Candy, S. M. Kaye, Y. Ren, R. E. Bell, G. W. Hammett, B. P. LeBlanc, D. R. Mikkelsen, W. M. Nevins, and H. Yuh, "Progress in simulating turbulent electron thermal transport in NSTX," Nucl. Fusion **53**(9), 093022 (2013).

[9]D. Told, F. Jenko, T. Görler, F. J. Casson, E. Fable, and ASDEX Upgrade Team, "Characterizing turbulent transport in ASDEX Upgrade l-mode plasmas via nonlinear gyrokinetic simulations," Phys. Plasmas **20**(12), 122312 (2013).

[10]A. R. Field, D. Dunai, Y. C. Ghim, P. Hill, B. McMillan, C. M. Roach, S. Saarelma, A. A. Schekochihin, S. Zoletnik, and MAST Team, "Comparison of BES measurements of ion-scale turbulence with direct gyro-kinetic simulations of mast l-mode plasmas," Plasma Phys. Controlled Fusion **56**(2), 025012 (2014).

[11]T. Görler, A. E. White, D. Told, F. Jenko, C. Holland, and T. L. Rhodes, "A flux-matched gyrokinetic analysis of DIII-D l-mode turbulence," Phys. Plasmas **21**(12), 122307 (2014).

[12]D. R. Mikkelsen, M. Bitter, L. Delgado-Aparicio, K. W. Hill, M. Greenwald, N. T. Howard, J. W. Hughes, J. E. Rice, M. L. Reinke, Y. Podpaly, Y. Ma, J. Candy, and R. E. Waltz, "Multispecies density peaking in gyrokinetic turbulence simulations of low collisionality Alcator C-Mod plasmas," Phys. Plasmas **22**(6), 062301 (2015).

[13]T. Happel, A. Bañón Navarro, G. D. Conway, C. Angioni, M. Bernert, M. Dunne, E. Fable, B. Geiger, T. Görler, F. Jenko, R. M. McDermott, F. Ryter, U. Stroth, and ASDEX Upgrade Team, "Core turbulence behavior moving from ion-temperature-gradient regime towards trapped-electron-mode regime in the ASDEX Upgrade tokamak and comparison with gyrokinetic simulation," Phys. Plasmas **22**(3), 032503 (2015).

[14]A. Bañón Navarro, T. Happel, T. Görler, F. Jenko, J. Abiteboul, A. Bustos, H. Doerk, D. Told, and ASDEX Upgrade Team, "Gyrokinetic studies of core turbulence features in ASDEX Upgrade H-mode plasmas," Phys. Plasmas **22**(4), 042513 (2015).

[15]W. Dorland, F. Jenko, M. Kotschenreuther, and B. N. Rogers, "Electron temperature gradient turbulence," Phys. Rev. Lett. **85**, 5579–5582 (2000).

[16]F. Jenko and W. Dorland, "Prediction of significant tokamak turbulence at electron gyroradius scales," Phys. Rev. Lett. **89**, 225001 (2002).

[17]F. Jenko, "On the nature of ETG turbulence and cross-scale coupling," J. Plasma Fusion Res. **6**, 11 (2004).

[18]R. E. Waltz, J. Candy, and M. Fahey, "Coupled ion temperature gradient and trapped electron mode to electron temperature gradient mode gyrokinetic simulations," Phys. Plasmas **14**(5), 056116 (2007).

[19]J. Candy, R. E. Waltz, M. R. Fahey, and C. Holland, "The effect of ion-scale dynamics on electron-temperature-gradient turbulence," Plasma Phys. Controlled Fusion **49**(8), 1209 (2007).

[20]T. Görler and F. Jenko, "Scale separation between electron and ion thermal transport," Phys. Rev. Lett. **100**, 185002 (2008).

[21]L. Schmitz, C. Holland, T. L. Rhodes, G. Wang, L. Zeng, A. E. White, J. C. Hillesheim, W. A. Peebles, S. P. Smith, R. Prater, G. R. McKee, Z. Yan, W. M. Solomon, K. H. Burrell, C. T. Holcomb, E. J. Doyle, J. C. DeBoo, M. E. Austin, J. S. deGrassie, and C. C. Petty, "Reduced electron thermal transport in low collisionality h-mode plasmas in DIII-D and the importance of TEM/ETG-scale turbulence," Nucl. Fusion **52**(2), 023003 (2012).

[22]N. T. Howard, A. E. White, M. Greenwald, C. Holland, and J. Candy, "Multi-scale gyrokinetic simulation of Alcator C-mod tokamak discharges," Phys. Plasmas **21**(3), 032308 (2014).

[23]S. Maeyama, Y. Idomura, T.-H. Watanabe, M. Nakata, M. Yagi, N. Miyato, A. Ishizawa, and M. Nunami, "Cross-scale interactions between electron and ion scale turbulence in a tokamak plasma," Phys. Rev. Lett. **114**, 255002 (2015).

[24]N. T. Howard, C. Holland, A. E. White, M. Greenwald, and J. Candy, "Fidelity of reduced and realistic electron mass ratio multi-scale gyrokinetic simulations of tokamak discharges," Plasma Phys. Controlled Fusion **57**(6), 065009 (2015).

[25]N. T. Howard, C. Holland, A. E. White, M. Greenwald, and J. Candy, "Synergistic cross-scale coupling of turbulence in a tokamak plasma," Phys. Plasmas **21**(11), 112510 (2014).

[26]N. T. Howard, C. Holland, A. E. White, M. Greenwald, and J. Candy, "Multi-scale gyrokinetic simulation of tokamak plasmas: Enhanced heat loss due to cross-scale coupling of plasma turbulence," Nucl. Fusion **56**(1), 014004 (2016).

[27]N. T. Howard, A. E. White, M. Greenwald, M. L. Reinke, J. Walk, C. Holland, J. Candy, and T. Görler, "Investigation of the transport shortfall in Alcator C-mod l-mode plasmas," Phys. Plasmas **20**(3), 032510 (2013).

[28]N. T. Howard, A. E. White, M. Greenwald, M. L. Reinke, C. Holland, J. Candy, and J. R. Walk, "Validation of the gyrokinetic model in ITG and TEM dominated L-mode plasmas," Nucl. Fusion **53**(12), 123011 (2013).

[29]J. Candy and R. E. Waltz, "Anomalous transport scaling in the DIII-D tokamak matched by supercomputer simulation," Phys. Rev. Lett. **91**, 045001 (2003).

[30]R. L. Miller, M. S. Chu, J. M. Greene, Y. R. Lin-Liu, and R. E. Waltz, "Noncircular, finite aspect ratio, local equilibrium model," Phys. Plasmas **5**(4), 973–978 (1998).

[31]A. Creely, A. E. White, E. Edlund, N. T. Howard, and A. Hubbard, "Perturbative thermal diffusivity from partial sawtooth crashes in alcator c-mod," Nuclear Fusion **56**, 036003 (2016).

[32]C. Holland, G. R. Tynan, R. J. Fonck, G. R. McKee, J. Candy, and R. E. Waltz, "Zonal-flow-driven nonlinear energy transfer in experiment and simulation," Phys. Plasmas **14**(5), 056112 (2007).

[33]Ch. P. Ritz and E. J. Powers, "Estimation of nonlinear transfer functions for fully developed turbulence," Phys. D **20**(2–3), 320–334 (1986).

[34]Ch. P. Ritz, E. J. Powers, and R. D. Bengtson, "Experimental measurement of three-wave coupling and energy cascading," Phys. Fluids B **1**(1), 153 (1989).

[35]C. Holland and P. H. Diamond, "A simple model of interactions between electron temperature gradient and drift-wave turbulence," Phys. Plasmas **11**(3), 1043–1051 (2004).

[36]T. S. Hahm, K. H. Burrell, Z. Lin, R. Nazikian, and E. J. Synakowski, "Zonal flow measurements concept I," Plasma Phys. Controlled Fusion **42**(5A), A205 (2000).

[37]G. M. Staebler, J. Candy, N. T. Howard, and C. Holland, "The role of zonal flows in the saturation of multi-scale gyrokinetic turbulence," Physics of Plasmas (submitted).

[38]J. C. DeBoo, C. C. Petty, A. E. White, K. H. Burrell, E. J. Doyle, J. C. Hillesheim, C. Holland, G. R. McKee, T. L. Rhodes, L. Schmitz, S. P. Smith, G. Wang, and L. Zeng, "Electron profile stiffness and critical gradient studies," Phys. Plasmas **19**(8), 082518 (2012).

[39]C. Holland, J. E. Kinsey, J. C. DeBoo, K. H. Burrell, T. C. Luce, S. P. Smith, C. C. Petty, A. E. White, T. L. Rhodes, L. Schmitz, E. J. Doyle, J.

C. Hillesheim, G. R. McKee, Z. Yan, G. Wang, L. Zeng, B. A. Grierson, A. Marinoni, P. Mantica, P. B. Snyder, R. E. Waltz, G. M. Staebler, and J. Candy, "Validation studies of gyrofluid and gyrokinetic predictions of transport and turbulence stiffness using the DIII-D tokamak," Nucl. Fusion **53**(8), 083027 (2013).

[40]J. C. Hillesheim, J. C. DeBoo, W. A. Peebles, T. A. Carter, G. Wang, T. L. Rhodes, L. Schmitz, G. R. McKee, Z. Yan, G. M. Staebler, K. H. Burrell, E. J. Doyle, C. Holland, C. C. Petty, S. P. Smith, A. E. White, and L. Zeng, "Experimental characterization of multiscale and multifield turbulence as a critical gradient threshold is surpassed in the DIII-D tokamak," Phys. Plasmas **20**(5), 056115 (2013).

[41]M. Greenwald, R. L. Boivin, F. Bombarda, P. T. Bonoli, C. L. Fiore, D. Garnier, J. A. Goetz, S. N. Golovato, M. A. Graf, R. S. Granetz, S. Horne, A. Hubbard, I. H. Hutchinson, J. H. Irby, B. LaBombard, B. Lipschultz, E. S. Marmar, M. J. May, G. M. McCracken, P. O'Shea, J. E. Rice, J. Schachter, J. A. Snipes, P. C. Stek, Y. Takase, J. L. Terry, Y. Wang, R. Watterson, B. Welch, and S. M. Wolfe, "H mode confinement in Alcator C-mod," Nucl. Fusion **37**(6), 793 (1997).

[42]J. C. Hillesheim, J. C. DeBoo, W. A. Peebles, T. A. Carter, G. Wang, T. L. Rhodes, L. Schmitz, G. R. McKee, Z. Yan, G. M. Staebler, K. H. Burrell, E. J. Doyle, C. Holland, C. C. Petty, S. P. Smith, A. E. White, and L. Zeng, "Observation of a critical gradient threshold for electron temperature fluctuations in the DIII-D tokamak," Phys. Rev. Lett. **110**, 045003 (2013).

[43]T. Görler and F. Jenko, "Multiscale features of density and frequency spectra from nonlinear gyrokinetics," Phys. Plasmas **15**(10), 102508 (2008).

[44]T. L. Rhodes, W. A. Peebles, X. Nguyen, J. C. Hillesheim, L. Schmitz, A. E. White, and G. Wang, "Quasioptical design of integrated Doppler backscattering and correlation electron cyclotron emission systems on the DIII-D tokamak," Rev. Sci. Instrum. **81**(10), 10D912 (2010).

[45]T. L. Rhodes, W. A. Peebles, M. A. Van Zeeland, J. S. deGrassie, R. V. Bravenec, K. H. Burrell, J. C. DeBoo, J. Lohr, C. C. Petty, X. V. Nguyen, E. J. Doyle, C. M. Greenfield, L. Zeng, and G. Wang, "Response of multi-scale turbulence to electron cyclotron heating in the DIII-D tokamak," Phys. Plasmas **14**(5), 056117 (2007).

[46]E. Mazzucato, D. R. Smith, R. E. Bell, S. M. Kaye, J. C. Hosea, B. P. LeBlanc, J. R. Wilson, P. M. Ryan, C. W. Domier, N. C. Luhmann, H. Yuh, W. Lee, and H. Park, "Short-scale turbulent fluctuations driven by the electron-temperature gradient in the national spherical torus experiment," Phys. Rev. Lett. **101**, 075001 (2008).

[47]D. R. Smith, S. M. Kaye, W. Lee, E. Mazzucato, H. K. Park, R. E. Bell, C. W. Domier, B. P. LeBlanc, F. M. Levinton, N. C. Luhmann, J. E. Menard, and H. Yuh, "Observations of reduced electron gyroscale fluctuations in national spherical torus experiment h-mode plasmas with large flow shear," Phys. Rev. Lett. **102**, 225005 (2009).

[48]T. L. Rhodes, W. A. Peebles, X. Nguyen, M. A. VanZeeland, J. S. deGrassie, E. J. Doyle, G. Wang, and L. Zeng, "Millimeter-wave backscatter diagnostic for the study of short scale length plasma fluctuations (invited)," Rev. Sci. Instrum. **77**(10), 10E922 (2006).

[49]Y. Ren, W. Guttenfelder, S. M. Kaye, E. Mazzucato, R. E. Bell, A. Diallo, C. W. Domier, B. P. LeBlanc, K. C. Lee, M. Podesta, D. R. Smith, and H. Yuh, "Electron-scale turbulence spectra and plasma thermal transport responding to continuous e × b shear ramp-up in a spherical tokamak," Nucl. Fusion **53**(8), 083007 (2013).

[50]J. Candy and R. E. Waltz, "An Eulerian gyrokinetic-Maxwell solver," J. Comput. Phys. **186**(2), 545–581 (2003).